Available online at www.sciencedirect.com
ScienceDirect
International Journal of Heat and Mass Transfer 51 (2008) 4447–4460
International Journal of HEAT and MASS TRANSFER
www.elsevier.com/locate/ijhmt

Solidification of a 2-D semitransparent medium using the lattice Boltzmann method and the finite volume method

Subhash C. Mishra *, Nikhil C. Behera, Atul K. Garg, Abhishek Mishra

Department of Mechanical Engineering, Indian Institute of Technology Guwahati, Guwahati 781039, India

Received 9 April 2007; received in revised form 4 February 2008
Available online 8 April 2008

Abstract

This article deals with the analysis of solidification of a 2-D semitransparent absorbing, emitting and scattering medium. An enthalpy based formulation was employed to simulate the phase-change process. Solidification was assumed to occur over a range of temperatures, and accordingly distinct liquid-, mushy- and solid-zones were considered. The problem was solved using the lattice Boltzmann method. The finite volume method was used to compute the radiative information required in the LBM formulation. Effects of various parameters such as the extinction coefficient, the scattering albedo, the conduction–radiation parameter and the latent heat were studied on temperature and liquid fraction distributions in the medium. These parameters were found to have significant effect on results.

Keywords: Solidification; Semitransparent medium; Lattice Boltzmann method; Finite volume method

1. Introduction

Numerical modeling of the solidification and melting phenomena is an important field of research because of its relevance in various engineering applications such as crystal growth, alloy processing, nuclear engineering and laser material processing [1–18]. Due to the complex mechanism governing formation and movement of the phase-change interface, the analytical solutions are limited to simple cases [1]. Numerical methods are more frequently used to analyze the phase-change process [2–18].

Semitransparent materials such as oxides, fluorides and silicon find extensive applications as single- and poly-crystals, glasses, ceramics and composites [19–24]. Unlike phase change of metals in which thermal radiation appears only in the boundary conditions, in semitransparent materials, it penetrates inside the medium and thus its consideration in the governing energy equation becomes essential [2–18]. Further, response of these materials towards absorption, emission and scattering of thermal radiation has considerable effect on the phase change process.

Different conventional CFD method such as the finite difference method, the finite element method and the finite volume method (FVM) have been used to analyze the phase-change processes of semitransparent materials [2–12]. In using these methods to solve the energy equation, the radiative information was computed using the methods like the P-1 approximation [5], the discrete ordinates method (DOM) [9–11,18] and the discrete transfer method (DTM) [17].

The lattice Boltzmann method [LBM] is relatively a new CFD tool to analyze various types of problems in science and engineering [14–18,25–33]. Because of its mesoscopic origin, it has several advantages. Some of these include simple calculation procedure, simple and efficient implementation for parallel computation, easy and robust handling of complex geometries and high computational performance with regard to stability and accuracy [25–27].

Recently the application of the LBM has been extended to simulate the phase-change process. Jiaung et al. [13] analyzed solidification of a planar layer using the LBM. Chatterjee and Chakraborty [15] used the LBM to solve

* Corresponding author. Tel.: +91 361 2582660; fax: +91 361 2690762.
E-mail address: scm_iitg@yahoo.com (S.C. Mishra).

0017-9310/$ - see front matter © 2008 Elsevier Ltd. All rights reserved.
doi:10.1016/j.ijheatmasstransfer.2008.02.003

Nomenclature

A	area (m^2)
b	number of directions in a lattice
c_p	specific heat (kJ/kg K)
C	heat capacity (kJ/m^3 K)
e_i	propagation speed in the direction i in the lattice, $\lvert\vec{e}_i\rvert$ (m/s)
$\vec{e}_i$	propagation velocity in the direction i in the lattice (m/s)
f_l	volume phase fraction of the liquid phase
G	incident radiation (W/m^2)
H	total enthalpy (kJ/kg)
I	intensity (W/m^2)
k	thermal conductivity (W/mK)
L	latent heat (kJ/kg)
M	total number of rays/intensities
N	conduction–radiation parameter $= \frac{k\beta}{4\sigma T_s^3}$
n_i	particle distribution function in the i-direction (K)
$n_i^{(0)}$	equilibrium particle distribution function in the i-direction (K)
q_R	radiative heat flux (W/m^2)
$\vec{r}$	lattice node (m)
S	radiative source term (W/m^2)
St	Stanton number $= \frac{C_s(T_0-T_N)}{L}$
T	temperature (K)
t	time (s)
V	volume (m^3)
w_i	weight factor corresponding to the direction i in a lattice
X, Y	x- and y-dimensions of the geometry (m)
x, y	coordinate directions

Greek symbols

α	thermal diffusivity (m^2/s)
β	extinction coefficient (m^{-1})
ε	emissivity
ρ	density (kg/m^3)
θ	polar angle
ϕ	azimuthal angle
σ	Stefan–Boltzmann constant $= 5.67 \times 10^{-8}$ W/m^2 K^4
τ	relaxation time (s)
$\Delta\Omega$	elemental solid angle
ω	scattering albedo
Φ	source term which affects the distribution function n_i, Eq. (26).

Subscripts

b	boundary
E, W, N, S	east, west, north, south
i	lattice direction index
0	initial temperature
l	liquid phase
m	melting
P	cell center
s	solid phase

Superscripts

K	iteration level at a given time level
m	direction index

solidification of a 3-D cubical medium. Their analyses were limited to solidification of metals which did not require consideration of volumetric radiation.

Very recently, Raj et al. [17] and Parida et al. [18] solved solidification of a 1-D planar semitransparent material using the LBM. Raj et al. [17] computed the radiative information using the DTM, while in [18], Parida et al. computed the same using the DOM. In references [17,18], the LBM in conjunction of the DTM or the DOM was found to successfully analyze the solidification process in a 1-D planar medium. Radiation was found to have significant effect on liquid-fraction and temperature distributions.

The 2-D geometries bring additional complications as unlike the 1-D planar medium, the mushy-zone spans over the 2-D space and the effect of all the four boundaries need to be taken into account. Further, radiation in this case is no longer azimuthally symmetric and the LBM has to be compatible with the method to calculate the radiative transfer.

To extend the application of the LBM, in the present work, we analyze solidification of a 2-D semitransparent material. An enthalpy based formulation is used to simulate the phase-change process. Solidification is assumed to occur over a range of temperatures, and accordingly distinct liquid-, mushy- and solid-zones are considered. Radiatively, the medium is considered absorbing, emitting and scattering. The radiative information required in the solution is computed using the FVM [33,34]. The mushy-zone interfaces are tracked and temperature profiles are computed for different parameters such as the extinction coefficient, the scattering albedo, the conduction–radiation parameter and the latent heat.

2. Formulation

Consider solidification of a 2-D rectangular semitransparent material (Fig. 1). Initially the material is at temperature T_0 which is higher than its melting temperature T_m. At time $t > 0$, its north boundary is maintained at temperature T_N which is below its melting temperature T_m. The remaining three boundaries are kept at initial temperature T_0. For the material under consideration, solidification is

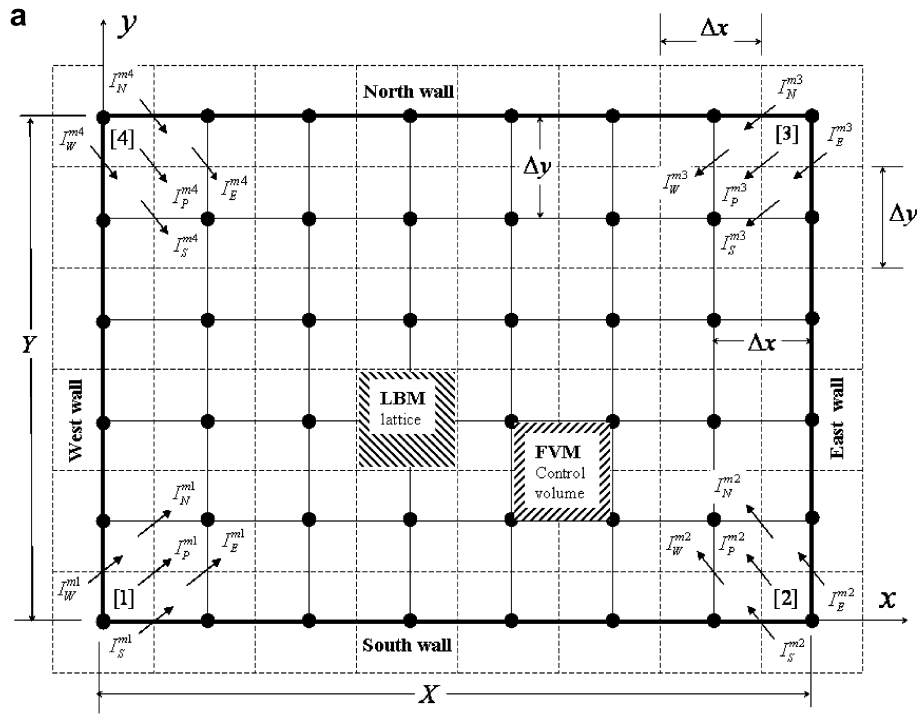

Quadrant	$\left(D_x^m, D_y^m\right)$
[1]	(+,+)
[2]	(-,+)
[3]	(-,-)
[4]	(+,-)

Fig. 1. (a) Arrangement of lattices and control volumes in a 2-D rectangular geometry with marching scheme in the FVM for four equally spaced sample directions with one in every quadrant and (b) coordinate system for direction in the FVM.

considered over a range of temperatures. With the passage of time, solidification starts from the north boundary and a mushy zone appears. Unlike the movement of a distinct front, the mushy-zone starts moving and its thickness changes with time. Further, since the material is a semi-transparent one, radiation penetrates inside and its consideration in the energy equation becomes paramount. For the problem under consideration, the enthalpy-based energy equation with volumetric radiation is

$$\frac{\partial(\rho H)}{\partial t} = -\nabla\cdot(-k\nabla T) - \nabla\cdot\vec{q}_{\mathrm{R}} \tag{1}$$

where H is the total enthalpy, ρ is the density, k is the thermal conductivity and $\vec{q}_{\mathrm{R}}$ is the radiative heat flux. In Eq. (1), for a 2-D rectangular medium (Fig. 1), $\nabla = \frac{\partial}{\partial x} + \frac{\partial}{\partial y}$. For a phase-change problem, the total enthalpy H is written as [1]

$$H = c_P T + f_{\mathrm{l}} L \tag{2}$$

where L is the latent heat and f_{l} is the liquid-fraction. In the solid-zone $f_{\mathrm{l}} = 0$, while for the liquid-zone $f_{\mathrm{l}} = 1$. In the mushy-zone, $0 < f_{\mathrm{l}} < 1$. With H defined as above, Eq. (1) can be written as

$$\frac{\partial(\rho c_P T)}{\partial t} = \nabla\cdot(k\nabla T) - L\frac{\partial(\rho f_{\mathrm{l}})}{\partial t} - \nabla\cdot\vec{q}_{\mathrm{R}} \tag{3}$$

If the thermophysical properties of the particular zone are assumed constant and also independent of time, we can write Eq. (3) for a specific (solid-, mushy- and liquid) zone as

$$\frac{\partial T}{\partial t} = \alpha\nabla^2 T - \frac{L}{C}\frac{\partial(\rho f_{\mathrm{l}})}{\partial t} - \frac{1}{C}\nabla\cdot\vec{q}_{\mathrm{R}} \tag{4}$$

where $\alpha = k/\rho c_P$ is the thermal diffusivity and $C = \rho c_p$ is the heat capacity. It is to be noted that α, C and ρ in differ-

ent zones have different values. In the solid-, mushy- and liquid-zones, the liquid-fraction f_l and enthalpy are related as [1]

$$f_l = \begin{cases} 0, & H < H_s \\ \frac{H-H_s}{H_l-H_s}, & H_s \leqslant H \leqslant H_l \\ 1, & H > H_l \end{cases} \quad (5)$$

In Eq. (5), subscripts s and l stand for solid- and liquid-zones, respectively. For the problem under consideration, the initial and the boundary conditions are the following:

$$\begin{aligned} &\text{Initial condition}: T(x,y,0) = T_0 > T_m \\ &\text{Boundary conditions}: T(x,0,t) = T_S = T_0 \\ &\qquad T(0,y,t) = T_W = T_0 \\ &\qquad T(X,y,t) = T_E = T_0 \\ &\qquad T(x,Y,t) = T_N < T_m \end{aligned} \quad (6)$$

In the present work, the LBM was used to solve the problem. The radiative information $\nabla \cdot \vec{q}_R$ required by the LBM was computed using the FVM. In the following pages, first we provide a brief formulation of the FVM to compute $\nabla \cdot \vec{q}_R$ followed by the LBM formulation to simulate the solidification process. The details of the FVM approach adopted in this work can be found in Mishra and Roy [33].

2.1. Finite volume method (FVM) formulation

The radiative transfer equation in any discrete direction $\hat{s}^m = (\sin\theta^m \cos\phi^m)\hat{i} + (\sin\theta^m \sin\phi^m)\hat{j} + (\cos\theta^m)\hat{k}$ with direction index m is given by

$$\frac{dI^m}{ds^m} = -\beta I^m + S^m \quad (7)$$

where I is the intensity and β is the extinction coefficient. The source term S for an absorbing, emitting and isotropically scattering medium is given by

$$S = \beta(1-\omega)\left(\frac{\sigma T^4}{\pi}\right) + \frac{\beta\omega}{4\pi} G \quad (8)$$

where ω is the scattering albedo and G is the incident radiation.

Resolving Eq. (7) along the x- and y-coordinate directions (Fig. 1b) and integrating it over the elemental solid-angle $\Delta\Omega^m$, we get

$$\frac{\partial I^m}{\partial x} D_x^m + \frac{\partial I^m}{\partial y} D_y^m = -\beta I^m \Delta\Omega^m + S^m \Delta\Omega^m \quad (9)$$

If $\hat{n}$ is the outward normal to a surface, then D^m is given by

$$D^m = \int_{\Delta\Omega^m} (\hat{n} \cdot \hat{s}^m)\, d\Omega \quad (10)$$

When the outward normal $\hat{n}$ is pointing towards one of the positive coordinate directions, D_x^m and D_y^m are given by [33]

$$D_x^m = \cos\phi^m \sin\left(\frac{\Delta\phi^m}{2}\right)[\Delta\theta^m - \cos 2\theta^m \sin(\Delta\theta^m)] \quad (11)$$

$$D_y^m = \sin\phi^m \sin\left(\frac{\Delta\phi^m}{2}\right)[\Delta\theta^m - \cos 2\theta^m \sin(\Delta\theta^m)] \quad (12)$$

For $\hat{n}$ pointing towards the negative coordinate directions, signs of D_x^m and D_y^m are opposite to what are obtained from Eqs. (11) and (12). In Eq. (9), $\Delta\Omega^m$ is given by [33]

$$\Delta\Omega^m = 2\sin\theta^m \sin\left(\frac{\Delta\theta^m}{2}\right)\Delta\phi^m \quad (13)$$

Integrating Eq. (9) over a 2-D control volume and using the concept of the FVM for the CFD, we get

$$[I_E^m - I_W^m]A_x D_x^m + [I_N^m - I_S^m]A_y D_y^m = [-\beta V I_P^m + V S_P^m]\Delta\Omega^m \quad (14)$$

where A_x and A_y are the areas of the x- and y-faces of the 2-D control volume, respectively. In Eq. (14), I with suffixes E, W, N and S designate east, west, north and south control surface average intensities, respectively. On the right-hand side of Eq. (14), $V = dx \times dy$ is the volume of the cell and I_P^m and S_P^m are the volume averaged intensity and source term at the cell centre P, respectively (Fig. 1a).

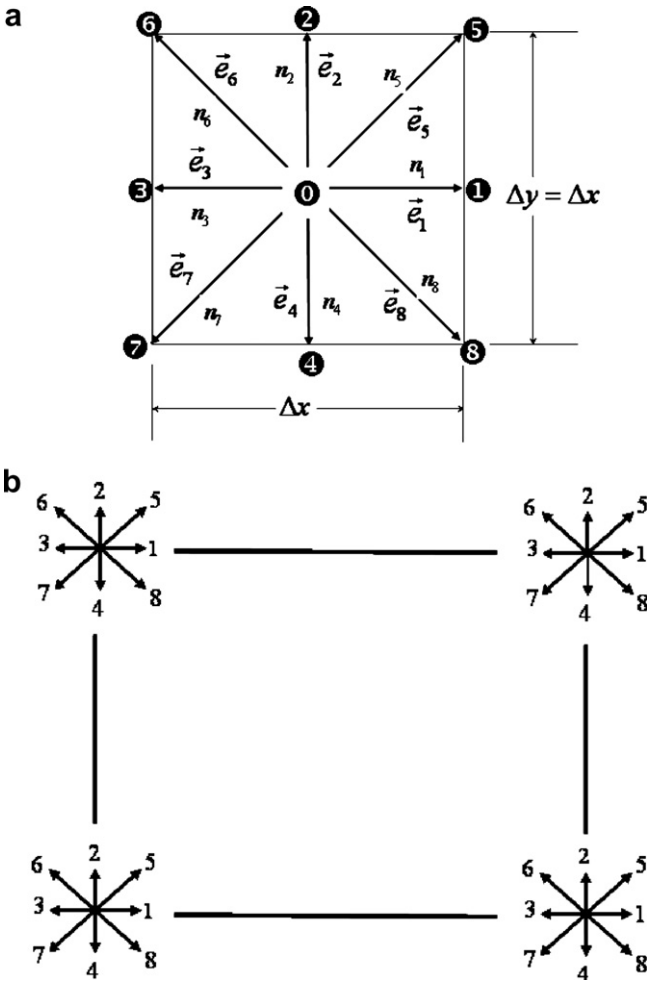

Fig. 2. (a) D2Q9 lattice used in a 2-D geometry and (b) schematic of particle distribution functions at the four corner points.

In any discrete direction having index m, the two cell-surface intensities and the cell-centre intensity I_P^m (Fig. 1a) can be related as

$$I_P^m = \frac{I_E^m + I_W^m}{2} = \frac{I_N^m + I_S^m}{2} \tag{15}$$

while marching from the first quadrant of a 2-D enclosure (Fig. 1a) for which D_x^m and D_y^m are both positive (Fig. 1b), from Eqs. (14) and (15), I_P^m in terms of known I_W^m, I_S^m and S_P^m is written as

$$I_P^m = \frac{2D_x^m A_x I_W^m + 2D_y^m A_y I_S^m + (V\Delta\Omega^m)S_P^m}{2D_x^m A_x + 2D_y^m A_y + \beta V \Delta\Omega^m},$$
$$\text{1st quadrant}: D_x^m > 0, \quad D_y^m > 0 \tag{16a}$$

while marching from other quadrants (Fig. 1a), either or both of D_x^m and D_y^m are negative (Fig. 1b). In this case, I_P^m in terms of known cell-surface intensities and source term is written as

$$I_P^m = \frac{2|D_x^m| A_x I_E^m + 2D_y^m A_y I_N^m + (V\Delta\Omega^m)S_P^m}{2|D_x^m| A_x + 2D_y^m A_y + \beta V \Delta\Omega^m},$$
$$\text{2nd quadrant}: D_x^m < 0, \quad D_y^m > 0 \tag{16b}$$

$$I_P^m = \frac{2|D_x^m| A_x I_E^m + 2|D_y^m| A_y I_N^m + (V\Delta\Omega^m)S_P^m}{2|D_x^m| A_x + 2|D_y^m| A_y + \beta V \Delta\Omega^m},$$
$$\text{3rd quadrant}: D_x^m < 0, \quad D_y^m < 0 \tag{16c}$$

$$I_P^m = \frac{2D_x^m A_x I_W^m + 2|D_y^m| A_y I_N^m + (V\Delta\Omega^m)S_P^m}{2D_x^m A_x + 2|D_y^m| A_y + \beta V \Delta\Omega^m},$$
$$\text{4 th quadrant}: D_x^m > 0, \quad D_y^m < 0 \tag{16d}$$

In Eq. (8), incident radiation G is numerically computed from the following [33]

$$G \approx \sum_{k=1}^{M_\phi} \sum_{l=1}^{M_\theta} I^m(\theta_l^m, \phi_k^m) 2 \sin\theta_l^m \sin\left(\frac{\Delta\theta_l^m}{2}\right) \Delta\phi_k^m \tag{17}$$

where M_θ and M_ϕ are the number of discrete points considered over the complete span of the polar angle ($0 \leqslant \theta \leqslant \pi$) and azimuthal angle ($0 \leqslant \phi \leqslant 2\pi$), respectively. Therefore,

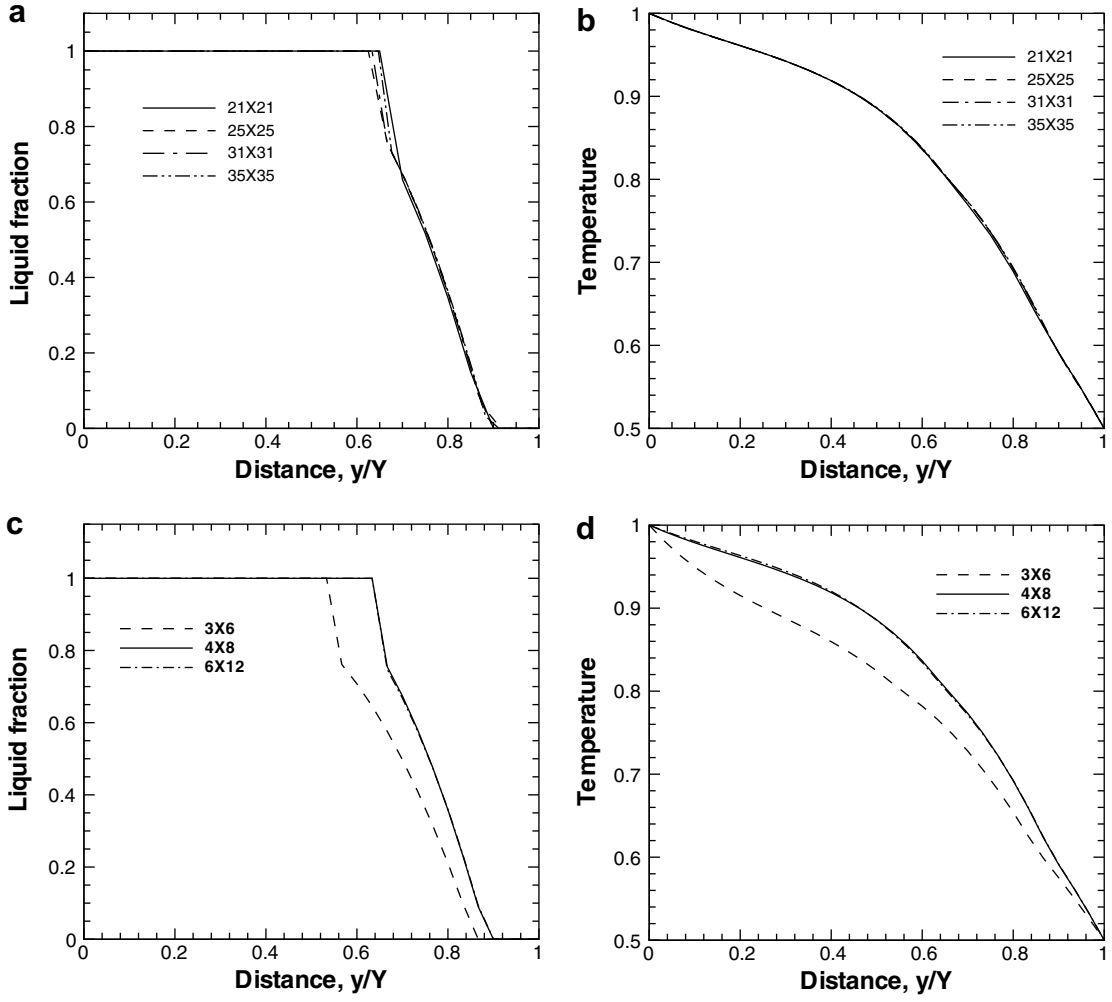

Fig. 3. Grid- and ray-independence tests: Effect of number of lattices/control volumes on centerline: (a) liquid-fraction and (b) temperature distributions for 4×8 rays. Effect of number of rays on centerline: (a) liquid-fraction and (b) temperature distributions for 31×31 lattices/control volumes.

$M_\theta \times M_\phi$ constitute the number of discrete directions in which intensities are considered at any point.

While marching from any of the corners, evaluation of Eq. (16) requires knowledge of the boundary intensity. For a diffuse-gray boundary having temperature T_b and emissivity ε_b, the boundary intensity I_b is computed from

$$I_b = \frac{\varepsilon_b \sigma T_b^4}{\pi} + \left(\frac{1-\varepsilon_b}{\pi}\right) \sum_{k=1}^{M_\phi} \sum_{l=1}^{M_\theta/2} I^m(\theta_l^m, \phi_k^m) \sin\theta_l^m \times \cos\theta_l^m \sin\Delta\theta_l^m \Delta\phi_k^m \quad (18)$$

In Eq. (18), the first and the second terms represent the emitted and the reflected components of the boundary intensity, respectively.

Once the intensity distributions are known, radiative information $\nabla \cdot \vec{q}_R$ required for the energy equation is computed from

$$\nabla \cdot \vec{q}_R = \beta(1-\omega)\left(4\pi \frac{\sigma T^4}{\pi} - G\right) \quad (19)$$

2.2. Lattice Boltzmann method (LBM) formulation

The discrete Boltzmann equation with Bhatanagar–Gross–Krook (BGK) approximation is given by [27]:

$$\frac{\partial n_i(\vec{r},t)}{\partial t} + \vec{e}_i \cdot \nabla n_i(\vec{r},t) = -\frac{1}{\tau}[n_i(\vec{r},t) - n_i^{(0)}(\vec{r},t)], \quad i = 0,1,2,\ldots,b \quad (20)$$

where n_i is the particle distribution function denoting the number of particles at the lattice node $\vec{r}$ and time t moving in direction i with velocity $\vec{e}_i$ along the lattice link $\Delta r = e_i \Delta t$ connecting the neighbors, $(b+1)$ is the number of particle distribution functions in a lattice (Fig. 2a) and b is the number of directions through which the information propagates. For the D2Q9 lattice (Fig. 2a), $b = 8$. In Eq. (20), τ is the relaxation time and $n_i^{(0)}$ is the equilibrium particle distribution function.

The relaxation time τ for the D2Q9 lattice (Fig. 2a) is computed from [27]

$$\tau = \frac{3\alpha}{|\vec{e}_i|^2} + \frac{\Delta t}{2} \quad (21)$$

where α is the thermal diffusivity and Δt is the time-step. The 9 velocities $\vec{e}_i$ and their corresponding weights w_i in the D2Q9 lattice (Fig. 2a) are the following [27]:

$$e_0 = (0,0), \quad e_{1,3} = (\pm 1, 0)\cdot U, \quad e_{2,4} = (0,\pm 1)\cdot U, \quad e_{5,6,7,8} = (\pm 1, \pm 1)\cdot U \quad (22)$$

$$w_0 = \frac{4}{9}, \quad w_{1,2,3,4} = \frac{1}{9}, \quad w_{5,6,7,8} = \frac{1}{36} \quad (23)$$

In Eq. (21), for a square lattice, $U = \frac{\Delta x}{\Delta t} = \frac{\Delta y}{\Delta t}$.

After discretization, Eq. (20) can be written as [27]

$$n_i(\vec{r} + \vec{e}_i \Delta t, t + \Delta t) = n_i(\vec{r},t) - \frac{\Delta t}{\tau}\left[n_i(\vec{r},t) - n_i^{(0)}(\vec{r},t)\right] \quad (24)$$

This is the LB equation with BGK approximation that describes the evolution of the particle distribution function n_i. Eq. (24) represents the equivalent of Eq. (4) without liquid-fraction (term 2) and the volumetric radiation (term 3) in the right hand side of the energy equation (Eq. (4)).

To account for the liquid-fraction (term 2) and volumetric radiation (term 3) in the right hand side of the energy equation (Eq. (4)), in the LBM formulation, Eq. (24) gets modified to [17,18,29–31,33]

$$n_i(\vec{r} + \vec{e}_i \Delta t, t + \Delta t) = n_i(\vec{r},t) - \frac{\Delta t}{\tau}[n_i(\vec{r},t) - n_i^{(0)}(\vec{r},t)] - \Delta t w_i \Phi_i - \left(\frac{\Delta t w_i}{C}\right)\nabla \cdot \vec{q}_R \quad (25)$$

where

$$\Phi_i = \frac{L\rho}{C}\left[\frac{f_l(\vec{r}, t+\Delta t) - f_l(\vec{r},t)}{\Delta t}\right]_i \quad (26)$$

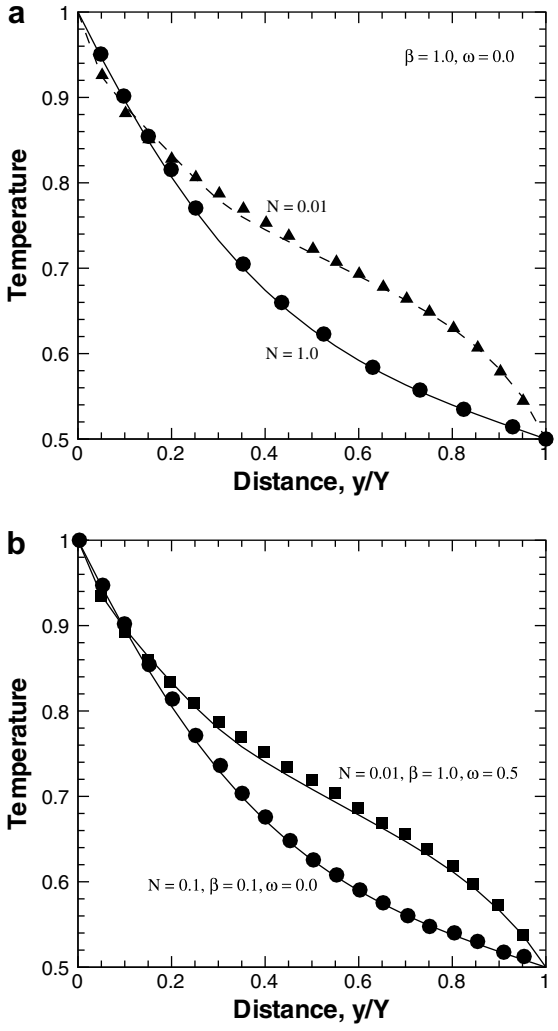

Fig. 4. Comparison of centerline temperature $\frac{T}{T_S}$ results of the present 2-D solidification code without phase change with that of [33]; Lines represent results of present work.

It is to be noted that the relaxation time τ, the density ρ and the heat capacity C are different for solid-, mushy- and liquid-zones.

Eq. (25) is the equivalent form of the energy equation (Eq. (4)) in the LBM formulation. It describes solidification of a semitransparent material taking place over a range of temperatures. It is to be noted that using the Chapman–Enskog multi-scale expansion, energy equation (Eq. (4)) can be deduced from Eq. (25). Further details on this for the solidification problem without and with radiation can be found in [13,16,17], respectively. For conduction–radiation problems without phase-change, the same can be found in [29–33].

For the problem under consideration, the temperature is obtained after summing the particle distribution functions n_i over all directions [27], i.e.,

$$T(\vec{r},t) = \sum_{i=0}^{8} n_i(\vec{r},t) \tag{27}$$

To process Eq. (25), the required equilibrium distribution function $n_i^{(0)}$ is given by

$$n_i^{(0)}(\vec{r},t) = w_i T(\vec{r},t) \tag{28}$$

For any lattice, the weights satisfy the relation $\sum_{i=0}^{8} w_i = 1$. Therefore, from Eqs. (27) and (28), we also have

$$\sum_{i=0}^{8} n_i^{(0)}(\vec{r},t) = \sum_{i=0}^{8} w_i T(\vec{r},t) = T(\vec{r},t) = \sum_{i=0}^{8} n_i(\vec{r},t) \tag{29}$$

2.3. Boundary conditions in the LBM and the FVM

In application of the LBM to heat transfer problems, temperature boundary condition can be applied using the bounce-back concept in which energy is balanced at any point on the boundary. Because of this balancing, in implementation of the LBM, as shown in Fig. 1a, the LBM lattices along the boundaries always extend a distance equal to half the control volume dimension in the respective coordinate directions and the lattice centres of the boundary lattices always lie along the boundaries. At each of the four corners, two directions that do not contribute to information propagation in the medium are not considered. For

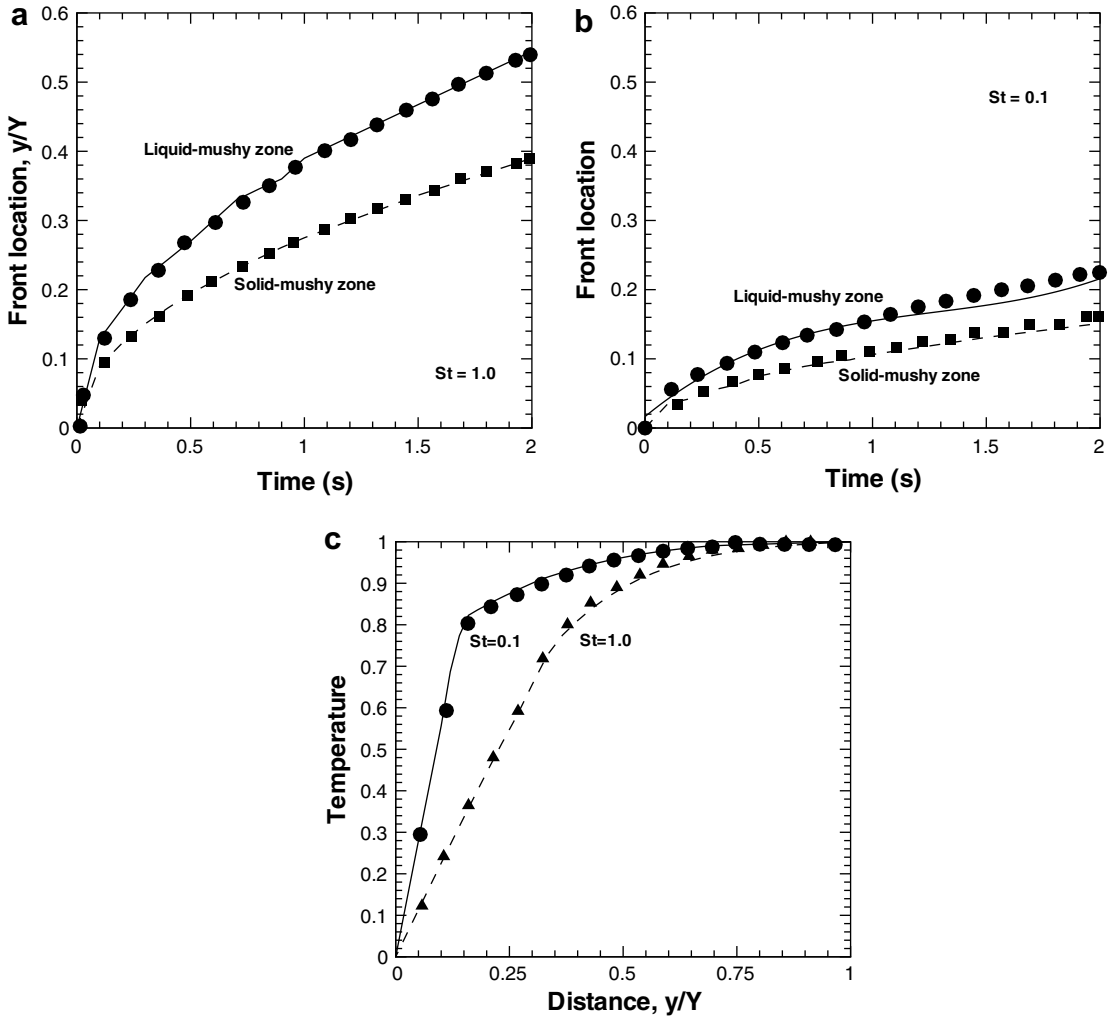

Fig. 5. Comparison of results of the 2-D LBM code for aspect ratio $\frac{X}{Y} = 10.0$ with 1-D analytic results: (a) front location with time for St = 1.0; (b) front location with time for St = 0.1 and (c) variation of temperature $\frac{T}{T_S}$ at time $t = 1.0$ s. Lines represent results of present work.

example, at the bottom-left and the top-right corners, directions 6 and 8 (Fig. 2b) and at the top-left and bottom-right corners directions 5 and 7 (Fig. 2b) have no influence and thus in the bounce-back scheme they are not considered. Details on implementation of the boundary conditions can be found in Mishra et al. [30].

In the solution of Eq. (25), radiative information $\nabla \cdot \vec{q}_R$ are required at the lattice centres. However, in the FVM, these are available only at the centres of the control surfaces and the control volumes (Fig. 1a). These values of $\nabla \cdot \vec{q}_R$ are translated to the lattice centres through an averaging procedure whose details can be found in Mishra and Roy [33].

Radiative boundary condition is required in determination of $\nabla \cdot \vec{q}_R$ that is needed in the solution of the energy equation (Eq. (25)). Eq. (18) is used in implementing the radiative boundary condition for a diffuse-gray wall at a prescribed wall temperature.

3. Solution procedure in the LBM

The medium is divided into a finite number of lattices/control volumes. The control volumes of the FVM for computing the radiative information $\nabla \cdot \vec{q}_R$ and lattices in the LBM are staggered as shown in Fig. 1a. Sizes of the lattices and the control volumes are taken the same. In solving Eq. (25), $\nabla \cdot \vec{q}_R$ information required at the lattice centres (Fig. 1a) are computed using the procedure described in Mishra et al. [33]. The algorithm for solving the solidification problem using the LBM is as follows.

1. Calculate the equilibrium particle distribution function $n_i^{(0)}(\vec{r},t)$ using Eq. (28) for the known temperature field. For the first time level, the particle distribution function is assumed as $n_i(\vec{r},t) = n_i^{(0)}(\vec{r},t)$.
2. Calculate the divergence of radiative heat flux $\nabla \cdot \vec{q}_R$ using Eq. (19).
3. For the Kth iteration, at the new time level $t + \Delta t$,
   a. Compute $n_i^K(\vec{r} + \vec{e}_i\Delta t, t + \Delta t)$

$$n_i^K(\vec{r}+\vec{e}_i\Delta t, t+\Delta t) = n_i(\vec{r},t) - \frac{\Delta t}{\tau(\vec{r})}[n_i(\vec{r},t) - n_i^{(0)}(\vec{r},t)] - \frac{\rho(\vec{r})L\Delta t w_i}{C(\vec{r})}\frac{f_l^{K-1}(\vec{r},t+\Delta t) - f_l(\vec{r},t)}{\Delta t} - \left(\frac{\Delta t w_i}{C(\vec{r})}\right)\nabla \cdot \vec{q}_R \quad (30)$$

   b. Compute temperature field $T^K(\vec{r},t)$ using Eq. (27).
   c. Compute the total enthalpy $H^K = CT^K + f_l^{K-1}L$.
   d. Update the liquid-fraction f_l^K using

$$f_l^K = \begin{cases} 0, & H^K < H_s \\ \frac{H^K - H_s}{H_l - H_s}, & H_s \leqslant H^K \leqslant H_l \\ 1, & H^K > H_l \end{cases} \quad (31)$$

   e. Check for convergence

$$\min\left(\left|\frac{f_l^K - f_l^{K-1}}{f_l^{K-1}}\right|, \left|\frac{T^K - T^{K-1}}{T^{K-1}}\right|\right) \leqslant 10^{-6}$$

   If converged, go to step 4. Else go to 3a.
4. At this time level $t + \Delta t$, propagate the particle distribution function n_i to the neighboring lattices and apply the boundary conditions.
5. Compute the new temperature field $T(\vec{r}, t + \Delta t)$ using Eq. (27).
6. Terminate the process when the desired time level or the steady-state is reached. Else go to step 1. For the steady-state the convergence criteria is:

$$\left|\frac{T(\vec{r},t+\Delta t) - T(\vec{r},t)}{T(\vec{r},t)}\right| \leqslant 10^{-6}$$

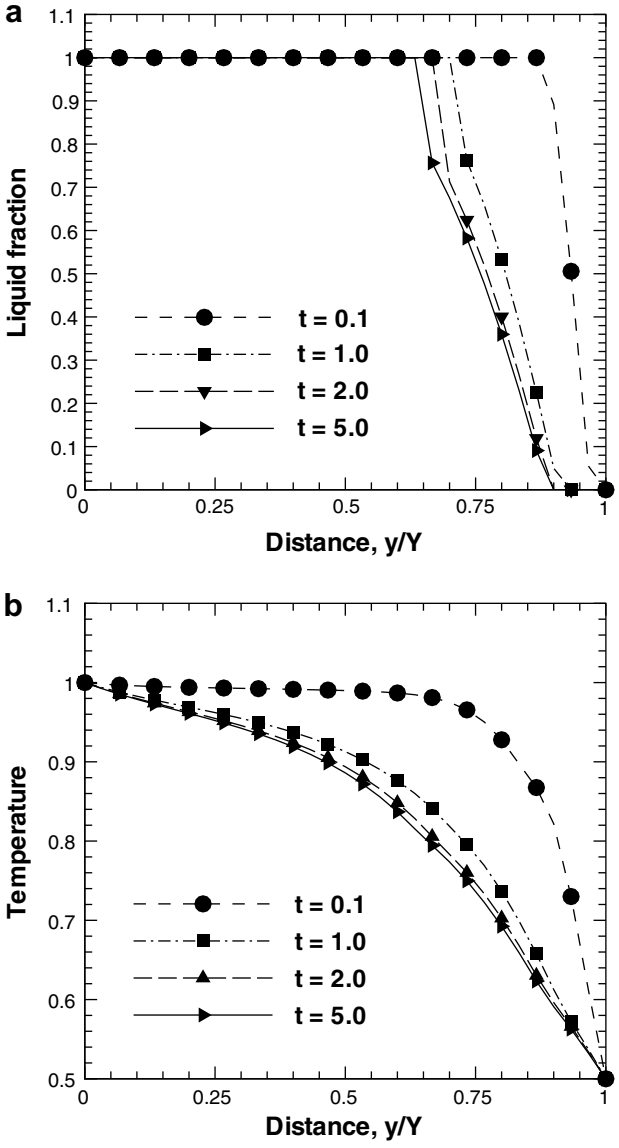

Fig. 6. Variation of centerline: (a) liquid-fraction f_l and (b) temperature T/T_S at different instants t; $\omega = 0.0$, $\beta = 1.0$, $N = 0.1$, $L = 1.0$.

4. Results and discussion

First the grid-independence and ray-independence studies were carried out for the LBM-FVM formulation presented in Section 2. Next, the 2-D LBM-FVM code for conduction–radiation without solidification was validated against Mishra et al. [35]. After that, by stretching one of the dimensions, the results from the present 2-D code for solidification without considering the effect of radiation were benchmarked against those available in the literature [1] for a 1-D planar medium. Then for different parameters such as the extinction coefficient β, the scattering albedo ω, the conduction–radiation parameter N and the latent heat L, liquid-fraction and temperature distributions in the medium were studied.

For a square medium undergoing solidification, grid-independence results are shown in Fig. 3a and b, and the ray-independence results are shown in Fig. 3c and d. With 4×8 rays, Fig. 3a and b, respectively show centreline $\left(\frac{x}{X} = 0.5\right)$ liquid-fraction f_l and temperature $\frac{T}{T_S}$ distributions along $\frac{y}{Y}$ for 21×21, 25×25, 31×31 and 35×35 lattices/control volumes. It is seen that the temperature distributions are independent of the lattices/control volumes considered. However, the results of the liquid-fraction have a slight variation in the mushy-zone. It is seen from Fig. 3a that 31×31 lattices/control volumes are optimum as no significant improvement beyond 31×31 lattices/control volumes is found.

With 31×31 lattices/control volumes, effects of different number of rays on centreline $\left(\frac{x}{X} = 0.5\right)$ liquid-fraction

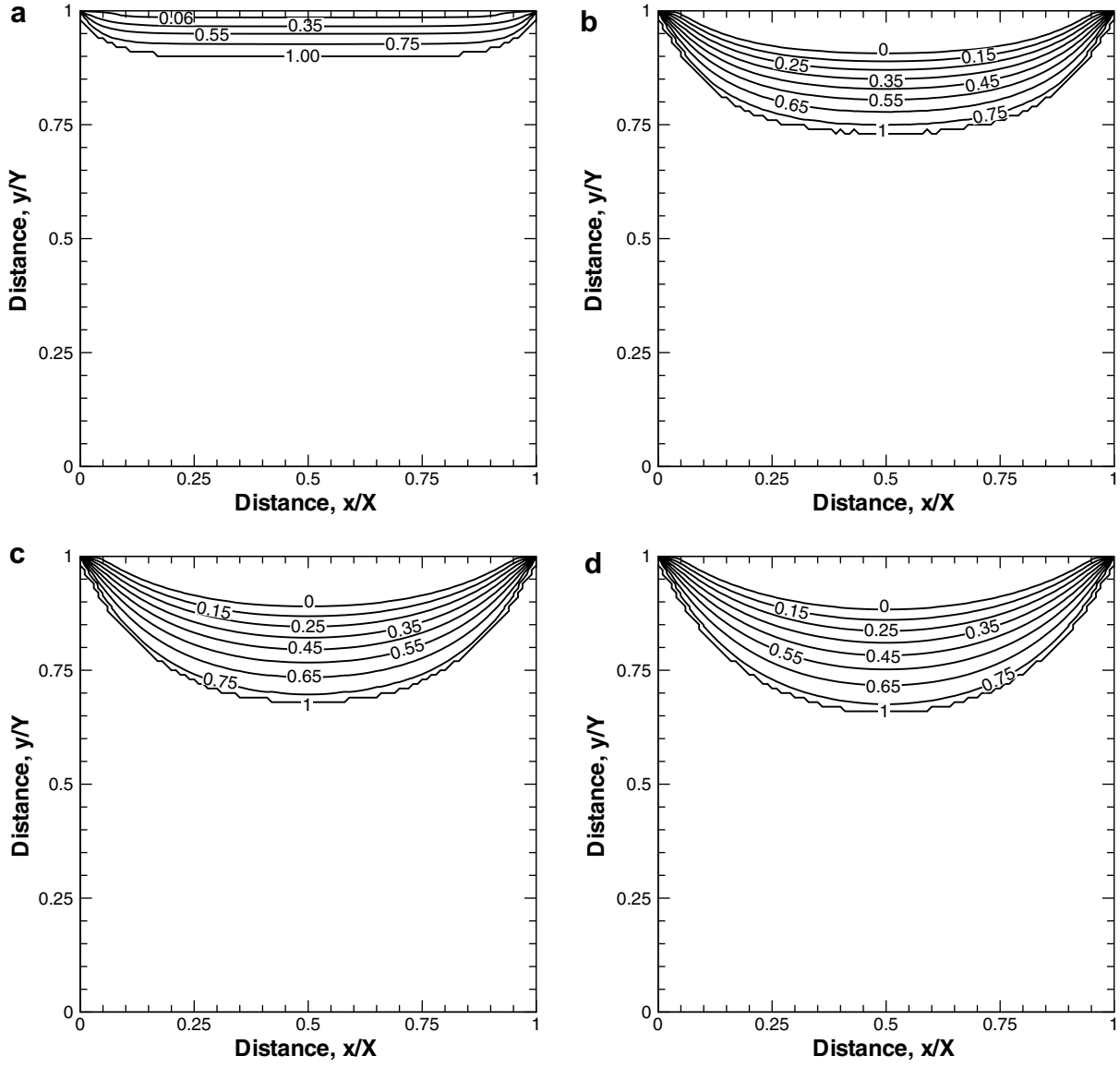

Fig. 7. liquid-fraction f_l contours at time (a) $t = 0.1$ s, (b) $t = 1.0$ s, (c) $t = 2.0$ s and (d) $t = 5.0$ s for $\omega = 0.0$, $\beta = 1.0$, $N = 0.1$, $L = 1.0$. In the mushy-zone $0 < f_l < 1$.

f_l and temperature $\frac{T}{T_S}$ distributions along $\frac{y}{Y}$ are shown in Fig. 3c and d, respectively. No significant change is observed beyond 4×8 rays. Thus in the following pages, for a 2-D square medium, all results are presented for 31×31 lattices/control volumes and 4×8 rays.

Fig. 4a and b show validation of the present 2-D LBM-FVM solidification code without considering the effect of phase-change with that reported in [35]. For this situation, the present problem reduces merely to an analysis of combined conduction and radiation heat transfer. In Fig. 4a, the present LBM-FVM centreline temperature $\frac{T}{T_S}$ results are compared for two values of the conduction–radiation parameter $N = 0.01$ and 1.0. With extinction coefficient $\beta = 1.0$, these comparisons are shown for absorbing-emitting case, $\omega = 0.0$. For $N = 0.1$, $\beta = 0.1$, $\omega = 0.0$ and $N = 0.01, \beta = 1.0, \omega = 0.5, \frac{T}{T_S}$ results are compared in Fig. 4b. It is seen from Fig. 4a and b that the results of the present work are in good agreement with those available in [34].

Fig. 5a–c show the validation of the present 2-D LBM-FVM solidification code without considering the effect of radiation. This validation is done with the analytic results of Co and Sunderland [1] for a 1-D planar medium. For this validation, the x-dimension of the 2-D medium in the present LBM-FVM code was stretched 10 times $\left(\frac{X}{Y} = 10\right)$ and then the results along the centreline $\left(\frac{x}{X} = 0.5\right)$ were compared with those of the 1-D case.

While validating the solidification results in Fig. 5a–c, the following material properties were kept the same as considered in [1]. $k_l/k_s = 0.6$, $k_{mz}/k_s = 0.76$, $C_l/C_s = 1.2$ and $C_{mz}/C_s = 1.12$. The numerical values of α for the three regions were calculated from the knowledge of the above ratios. The temperatures $\frac{T}{T_S}$ at the solid-mushy and mushy-liquid interfaces were set at 0.6 and 0.8, respec-

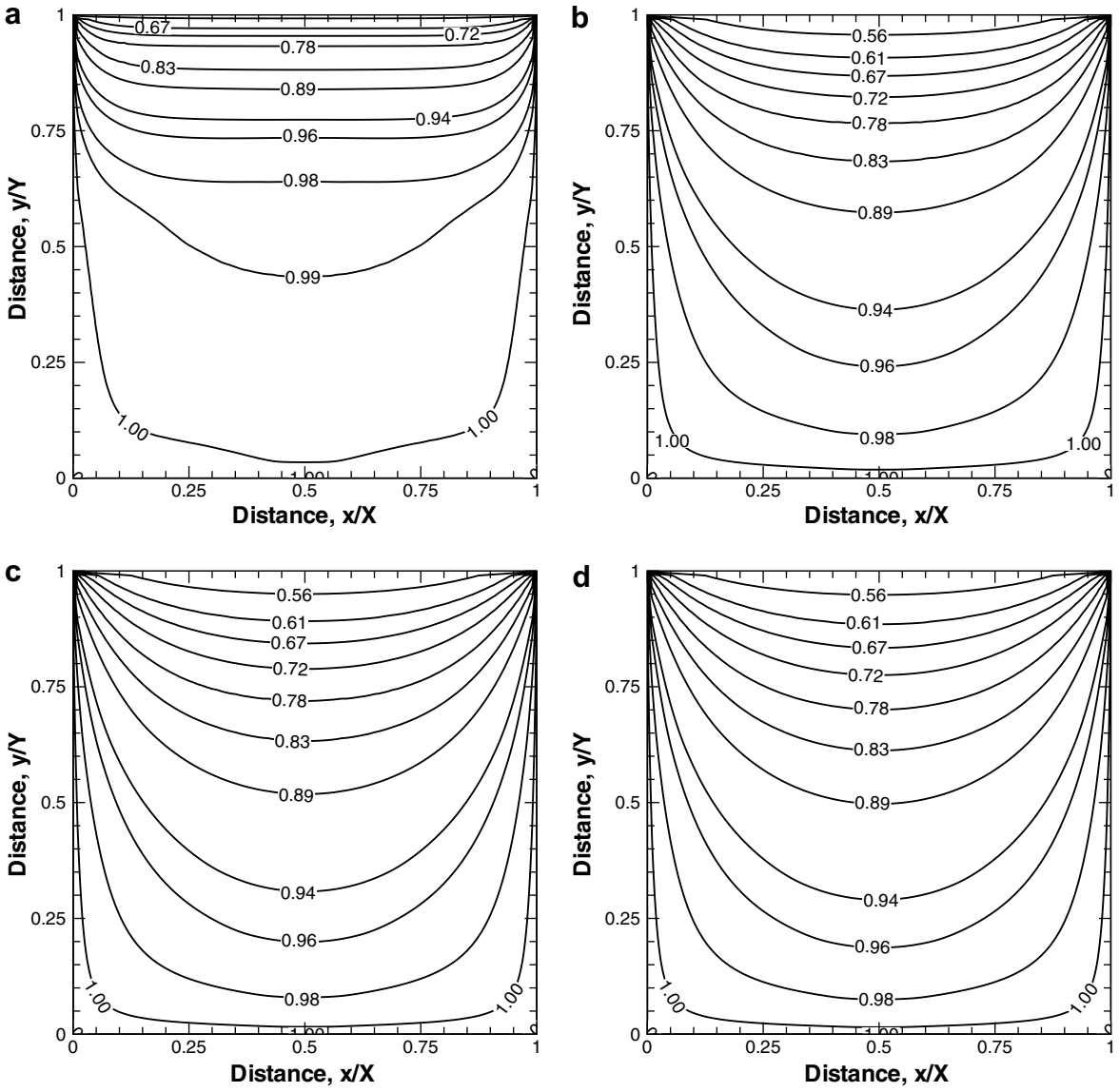

Fig. 8. Temperature T/T_S contours at time (a) $t = 0.1$ s, (b) $t = 1.0$ s, (c) $t = 2.0$ s and (d) $t = 5.0$ s for $\omega = 0.0$, $\beta = 1.0$, $N = 0.1$, $L = 1.0$.

tively. The initial temperature for this validation was taken as $\frac{T_0}{T_S} = 1.0$ and the boundary conditions for $t > 0$, were $\frac{T_W}{T_S} = \frac{T_E}{T_S} = 1.0$ and $\frac{T_N}{T_S} = 0.0$.

In Fig. 5a and b, movements of the solid-mushy and liquid-mushy fronts with time have been compared for Stanton number $St[= C_s(T_0 - T_N)/L] = 1.0$ and 0.1, respectively. In Fig. 5c, temperature $\frac{T}{T_S}$ distributions along the centreline have been compared for $St = 1.0$ and 0.1. It is seen from this figure that for $\frac{X}{Y} = 10.0$, the LBM-FVM 2-D results compare very well with 1-D analytic results given in [1].

In the following pages, while presenting the solidification results for a square medium $\left(\frac{X}{Y} = 1.0\right)$ with the effect of thermal radiation, the parameters were kept the same as considered in the validation of solidification results. The value of the solid thermal diffusivity α_s was obtained from the chosen values of the conduction–radiation parameter $N\left(= \frac{k\beta}{4\sigma T_S^3}\right)$ and the extinction coefficient β. The initial condition was set to $\frac{T_0}{T_S} = 1.0$. Since the temperature of 0.0 K is impractical in the problems involving radiation, for $t > 0$, the boundary conditions were kept as: $\frac{T_W}{T_S} = \frac{T_E}{T_S} = 1.0$ and $\frac{T_N}{T_S} = 0.5$. In calculation of the radiative information $\nabla \cdot \vec{q}_R$, all the four boundaries were assumed black.

Fig. 6a and b show the centreline liquid-fraction f_l and temperature $\frac{T}{T_S}$ distributions for an absorbing-emitting medium ($\omega = 0.0$) with $\beta = 1.0$, $N = 0.1$ and $L = 1.0$ kJ/kg over a period of 5 s. Fig. 7a–d show the liquid-fraction f_l contours in the three zones at time $t = 0.1$, 1.0, 2.0 and 5.0 s. In Fig. 8a–d, temperature $\frac{T}{T_S}$ contours are shown.

It is seen from Figs. 6a and 7a– d that with the passage of time, the thickness of the mushy-zone penetrates

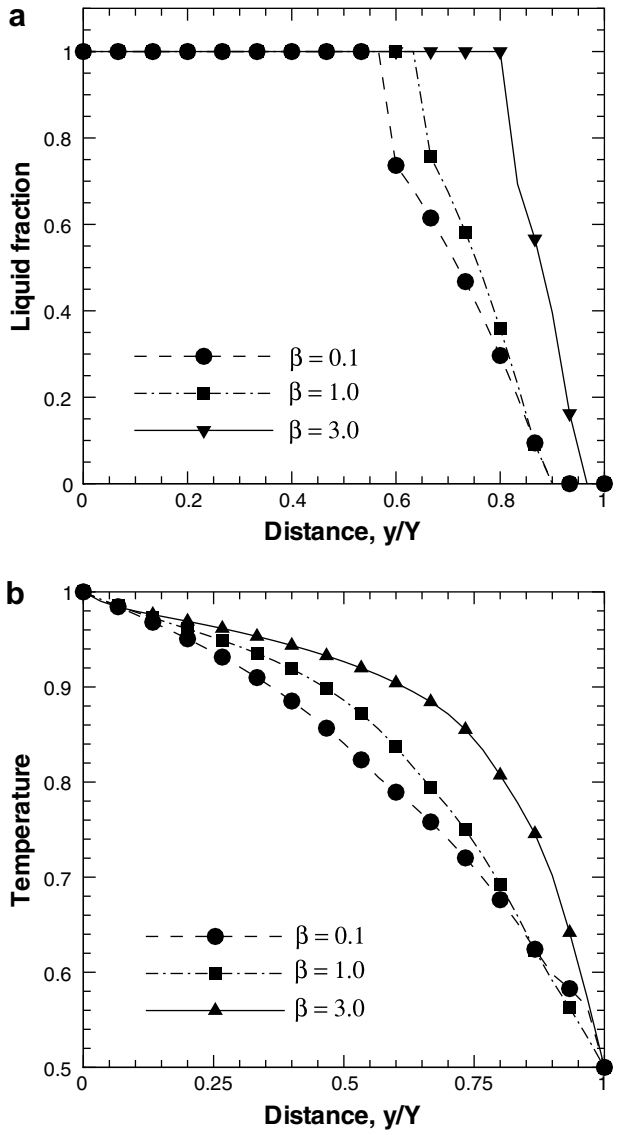

Fig. 9. Variation of centerline: (a) liquid-fraction f_l and (b) temperature T/T_S for different values of the extinction coefficient β at time $t = 5.0$ s; $\omega = 0.0$, $N = 0.1$, $L = 1.0$.

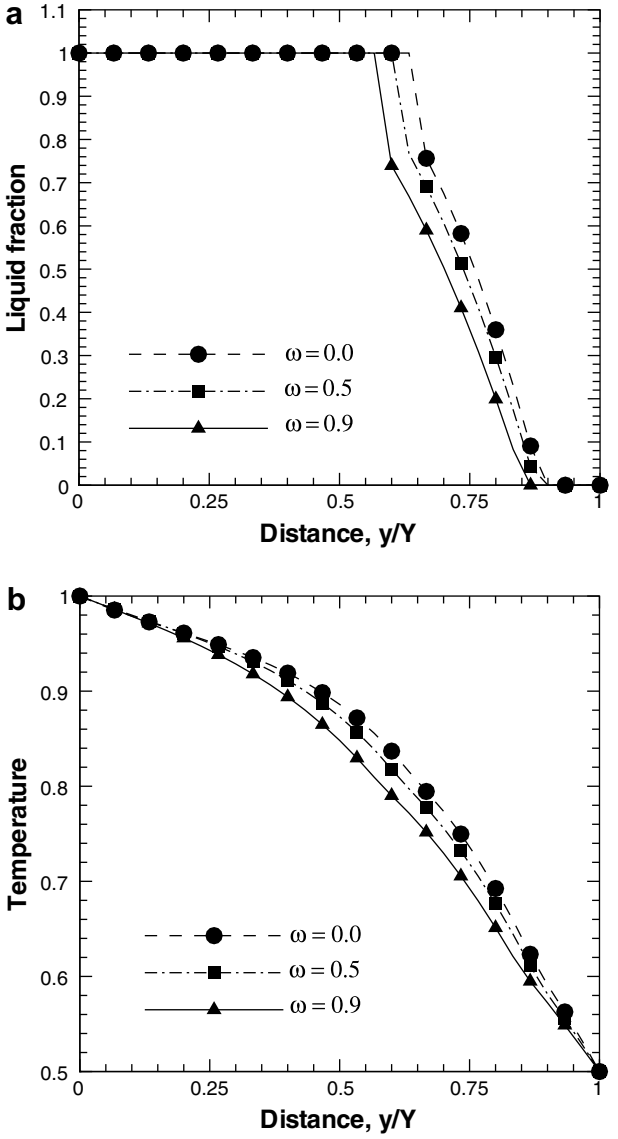

Fig. 10. Variation of centerline: (a) liquid-fraction f_l and (b) temperature T/T_S for different values of the scattering albedo ω at time $t = 5.0$ s; $\beta = 1.0$, $N = 0.1$, $L = 1.0$.

towards the south boundary and its thickness increases. Its thickness is maximum along the centreline $\left(\frac{x}{X}=0.5\right)$ and decreases symmetrically towards the east or the west boundary. It is observed from these figures that in the early stage, the mushy-zone grows at a faster rate.

It is seen from Figs. 6b and 8a–d that at any time, the temperature gradient is always more towards the cold boundary from where the solidification starts. With the passage of time, at any location, the temperature gradient decreases. In the mushy-zone, the gradient decreases from the solid-mushy interface to mushy-liquid interface. The reason for the decrease in temperature gradient with the passage of time is attributed to the fact that the cooling effect penetrates inside the medium with less intensity.

With $\omega=0.0$, $N=0.1$ and $L=1.0$ kJ/kg at time $t=5.0$ s, effect of the extinction coefficient β on the centreline liquid fraction f_l and temperature $\frac{T}{T_S}$ distributions is shown in Fig. 9a and b, respectively. It is seen from Fig. 9a that the mushy-zone thickness is less when the medium is radiatively more participating ($\beta=3.0$) and accordingly, as seen from Fig. 9b, the gradient in $\frac{T}{T_S}$ is more for this case ($\beta=3.0$). This trend is because of the fact that for a higher value of β, penetration of radiation in the medium is less because of high absorption. Thus the mushy zone moves slowly and also its thickness is less.

The effect of the scattering albedo ω on the centreline liquid fraction f_l and temperature $\frac{T}{T_S}$ distributions is shown in Figs. 10a and b, respectively. This effect is shown for $\beta=1.0$, $N=0.1$ and $L=1.0$ kJ/kg at time $t=5.0$ s. With increase in ω, the thickness of the mushy-zone increases and the temperature gradient decreases. This is because of the fact that with increase in ω, medium scatters more

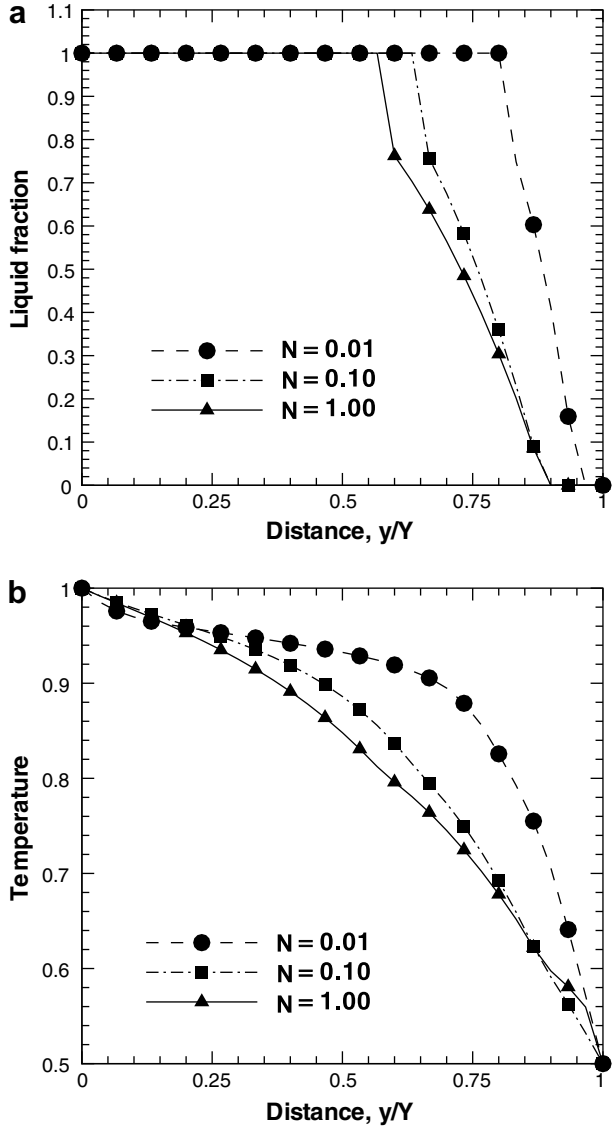

Fig. 11. Variation of centerline: (a) liquid-fraction f_l and (b) temperature T/T_S for different values of the conduction radiation parameter N at time $t=5.0$ s; $\beta=1.0$, $\omega=0.0$, $L=1.0$.

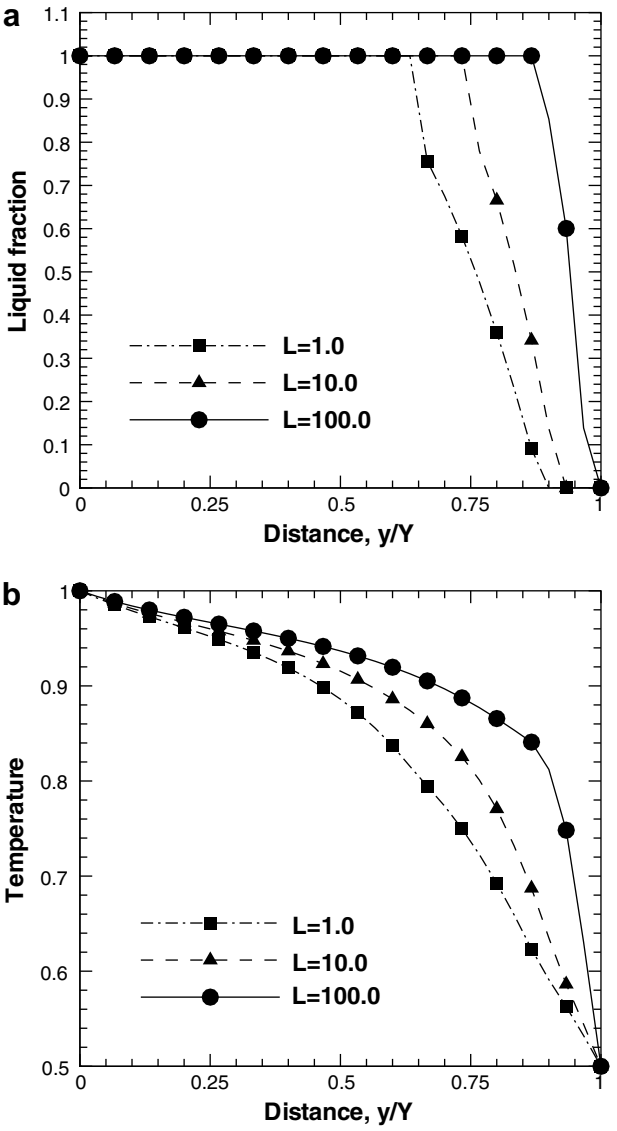

Fig. 12. Variation of centerline: (a) liquid-fraction f_l and (b) temperature T/T_S for different values of the latent heat L at time $t=5.0$ s; $\beta=1.0$, $\omega=0.0$, $N=0.1$.

energy and as seen from Eq. (19), the effect of radiation decreases.

Fig. 11a and b show the effect of the conduction–radiation parameter N on the centreline liquid-fraction f_l and temperature $\frac{T}{T_S}$ distributions, respectively. These results are shown for $\beta = 1.0$, $\omega = 0.0$ and $L = 1.0$ kJ/kg at time $t = 5.0$ s. It is observed that in the radiation dominated situation ($N = 0.01$), the mushy-zone thickness is less and its movement is also slow. In the mushy-zone, the temperature gradient is more in the radiation dominated case. Since the radiative contribution is of the order of σT_S^4, the radiation dominated case brings more non-linearity in the temperature profile. A similar trend with regard to the radiation effect has been found in Figs. 9 and 10 for $\beta = 3.0$ and $\omega = 0.0$, respectively.

Effect of the latent heat L on the centreline liquid-fraction f_l and temperature $\frac{T}{T_S}$ distributions are shown in Fig. 12a and b, respectively. At time $t = 5.0$ s, these results are shown for $\beta = 1.0$, $\omega = 0.0$ and $N = 0.1$. A high value of L implies that more energy has to be extracted to cause solidification and thus for this case, as observed from Fig. 12a, the mushy-zone thickness is less and its movement is slow. Further, as seen from Fig. 12b, the temperature gradient is also more when L is large.

All the computations in the present work were carried out with $\Delta t = 0.001$. The steady-state condition was observed at $t = 5$ s. Thus, all the runs were taken for 5000 iterations. On a CPU (512 MB, 2.8 GHz with hyper threading) the runs for various cases ranged from 25 to 40 min.

5. Conclusions

Solidification of a 2-D square semitransparent medium was analyzed using the LBM. An enthalpy based formulation was used to simulate the solidification process. Radiatively, the medium was considered absorbing, emitting and isotropically scattering. The radiative information was computed using the FVM. The results of the present 2-D LBM-FVM code were validated with those available in the literature. Firstly it was validated with the results of a 2-D conduction–radiation problem without phase change and then with a 1-D planar medium with phase change and without radiation by stretching one of its dimensions. Distributions of liquid-fractions and temperature were studied for different parameters such as the extinction coefficient, the scattering albedo, the conduction–radiation parameter and the latent heat. For a given set of parameters, evolution of liquid-fraction and temperature were also studied. It was found that in radiation dominated cases, which were identified with higher value of the extinction coefficient, lower value of the scattering albedo and lower value of the conduction–radiation parameter, the thickness of the mushy-zone was less, its movement was slow and the non-linearity in the temperature was comparatively more. A similar trend was also observed for a higher value of the latent heat.

References

[1] S.H. Co, J.E. Sunderland, Heat conduction problems with melting or freezing, J. Heat Transfer 91 (1969) 421–426.

[2] I.S. Habib, Solidification of semitransparent materials by conduction and radiation, Int. J. Heat Mass Transfer 14 (1971) 2161–2164.

[3] M. Abrams, R. Viskanta, The effects of radiative heat transfer upon the melting and solidification of semitransparent crystals, J. Heat Transfer 96 (1974) 184–190.

[4] S.H. Chan, D.H. Cho, G. Kocamustafaogullari, Melting and solidification with internal radiative transfer – a generalized phase change model, Int. J. Heat Mass Transfer 26 (1983) 621–633.

[5] F.O. Oruma, M.N. Ozisik, M.A. Boles, Effects of anisotropic scattering on melting and solidification of a semiinfinite semitransparent medium, Int. J. Heat Mass Transfer 28 (1985) 441–449.

[6] K.S. Kim, B. Yimer, Thermal radiation heat transfer effects on solidification of finite concentric cylindrical medium–enthalpy model and P-1 approximation, Numer. Heat Transfer 14 (1988) 483–498.

[7] V.S. Yuferev, Z. Chvoj, E.N. Kolesnikova, The effect of radiative heat transfer on morphological stability during directional solidification of a binary melt, J. Cryst. Growth 108 (1991) 367–376.

[8] B. Yimer, Multi-dimensional solidification with internal radiation and temperature dependent properties, Energy Convers. Manage. 41 (2000) 343–352.

[9] J.Y. Murthy, S.R. Mathur, A finite-volume scheme for radiative heat transfer in semitransparent media, Numer. Heat Transfer B 37 (2000) 25–43.

[10] C. Yao, B.T.F. Chung, Transient heat transfer in a scattering–radiating–conducting layer, J. Thermophys. Heat Transfer 13 (1999) 18–24.

[11] C. Yao, G.X. Wang, B.T.F. Chung, Nonequilibrium planar interface model for solidification of semitransparent radiating materials, J. Thermophys. Heat Transfer 14 (2000) 297–304.

[12] I. Anteby, I. Shai, A. Arbel, Numerical calculations for combined conduction and radiation transient heat transfer in a semitransparent medium, Numer. Heat Transfer A 37 (2000) 359–371.

[13] W.S. Jiaung, J.R. Ho, C.P. Kuo, Lattice Boltzmann method for heat conduction problem with phase change, Numer. Heat Transfer B 39 (2001) 167–187.

[14] Y. Shu, B.Q. Al, L. A1, K.G. Lynn, Numerical modeling of internal radiation and solidification in semitransparent melts in magnetic fields, Numer. Heat Transfer B 45 (2004) 957–976.

[15] D. Chatterjee, S. Chakraborty, An enthalpy-based lattice Boltzmann model for diffusion dominated solid–liquid phase transformation, Phys. Lett. A 341 (2005) 320–330.

[16] C.C. Tseng, R. Viskanta, Melting of a semitransparent bed of particles by convection and radiation, J. Am. Ceram. Soc. 89 (2006) 2547–2554.

[17] R. Raj, A. Prasad, P.R. Parida, S.C. Mishra, Analysis of solidification of a semitransparent planar layer using the lattice Boltzmann method and the discrete transfer method, Numer. Heat Transfer A 49 (2006) 279–299.

[18] P.R. Parida, R. Raj, A. Prasad, S.C. Mishra, Solidification of a semitransparent planar layer subjected to radiative and convective cooling, J. Quant. Spectros. Radiat. Transfer 107 (2007) 226–235.

[19] E.M. Genies, M. Lapkowski, C. Santier, E. Vieil, Polyaniline, spectrochemistry, display and battery, Synth. Met. 18 (1987) 631–636.

[20] B. Scosati, Conducting polymers: new frontiers and prospective, Mater. Sci. Eng. 12 (1992) 369–373.

[21] V.P. Petrov, Optical and thermophysical properties of semitransparent materials in the calculation of combined radiation-conduction heat transfer, Sov. Tech. Rev. B: Therm. Phys. 4 (1973) 1–79.

[22] J. Chen, A.K. Burrell, G.E. Callis, D. L Officer, G.F. Swiegers, Preparation, characterization and biosensor application of conditioning polymers based on ferrocene substituated thiopene and terthiophene, Electrochim. Acta 47 (2002) 2715–2724.

[23] K. Gurunathan, D. Amalnerkar, D. Triovedi, Synthesis and characterization of conducting polymer composite for cathode material in rechargeable battery, Mater. Lett. 57 (2003) 1642–1648.
[24] P. Sadooghi, Transient coupled radiative and conductive heat transfer in a semitransparent layer of ceramic, J. Quant. Spectros. Radiat. Transfer 92 (2005) 403–416.
[25] S. Chen, G.D. Doolen, Lattice Boltzamann method for fluid flows, Annu. Rev. Fluid Mech. 30 (1998) 329–364.
[26] X. He, S. Chen, G.D. Doolen, A novel thermal model for the lattice Boltzmann method in incompressible limit, J. Comput. Phys. 146 (1998) 282–300.
[27] S. Succi, The Lattice Boltzmann Method for Fluid Dynamics and Beyond, Oxford University Press, 2001.
[28] J.R. Ho, C.-P. Kuo, W.-S. Jiaung, C.–J. Twu, Lattice Boltzmann scheme for hyperbolic heat conduction equation, Numer. Heat Transfer B 41 (2002) 591–607.
[29] S.C. Mishra, A. Lankadasu, Analysis of transient conduction and radiation heat transfer using the lattice Boltzmann method and the discrete transfer method, Numer. Heat Transfer, A 47 (2005) 935–954.
[30] S.C. Mishra, A. Lankadasu, K. Beronov, Application of the lattice Boltzmann method for solving the energy equation of a 2-D transient conduction-radiation problem, Int. J. Heat Mass Transfer 48 (2005) 3648–3659.
[31] N. Gupta, G.R. Chaitanya, S.C. Mishra, Lattice Boltzmann method applied to variable thermal conductivity conduction and radiation problems, J. Thermophys. Heat Transfer 20 (2006) 895–902.
[32] T. Kush, B.S.R. Krishna, S.C. Mishra, Comparisons of the lattice Boltzmann method and the finite difference methods for heat conduction problems, in: S.C. Mishra, B.V.S.S.S. Prasad, S.V. Garimella (Eds.), Proceedings of 18th National & 7th ISHMT-ASME Heat and Mass Transfer Conference, Guwahati, India, 2006, Tata McGraw Hill, New Delhi, 2006 (Paper Number: HMT-2006-C012).
[33] S.C. Mishra, H.K. Roy, Solving transient conduction-radiation problems using the lattice Boltzmann method and the finite volume method, J. Comput. Phys. 233 (2007) 89–107.
[34] J.C. Chai, S.V. Patankar, Finite volume method for radiation heat transfer, Adv. Numer. Heat Transfer 2 (2000) 110–135.
[35] S.C. Mishra, P. Talukdar, D. Trimis, F. Durst, Computational efficiency improvements of the radiative transfer problems with or without conduction – a comparison of the collapsed dimension method and the discrete transfer method, Int. J. Heat Mass Transfer 46 (2003) 3083–3095.